Journal of Applied Fluid Mechanics, Vol. 11, No. 3, pp. 801-816, 2018.
Available online at www.jafmonline.net, ISSN 1735-3572, EISSN 1735-3645.
DOI: 10.29252/jafm.11.03.27945

Lattice Boltzmann Numerical Investigation of Inner Cylindrical Pin-fins Configuration on Nanofluid Natural Convective Heat Transfer in Porous Enclosure

Y. Jafari[1, 4], M. Taeibi-Rahni[2, 4†], M. Haghshenas[3] and P. Ramian[1]

[1] *Department of Mechanical Engineering, Central Tehran Branch, Islamic Azad Univ., Tehran, Iran*
[2] *Department of Aerospace Engineering, Sharif Univ., Tehran, P.O.B. 113658539, Iran*
[3] *Department of Mechanical and Aerospace Engineering, University of Central Florida, USA*
[4] *Aerospace Research Institute, Tehran, Iran*

†*Corresponding Author Email: taeibi@sharif.edu*

(Received May 3, 2017; accepted December 18, 2017)

ABSTRACT

Concerning the geometrical effect of inner cylindrical hot pins, the natural convective heat transfer of nanofluid in a homogenous porous medium in a squared enclosure is numerically studied, using lattice Boltzmann method (LBM). In order to investigate the arrangement of inner cylinders for better heat transfer performance, five different configurations (including one, three, and four pins) were compared, while the total heat transfer area of inner pins were held fixed. Squared cavity walls and inner cylinder's surfaces were constantly held at cold and warm temperatures, respectively. In our simulation, Brinkman and Forchheimer-extended Darcy models were utilized for isothermal incompressible flow in porous media. The flow and temperature fields were simulated using coupled flow and temperature distribution functions. The effect of porous media was added as a source term in flow distribution functions. The results were validated using previous creditable data, showing relatively good agreements. After brief study of copper nano-particles volume fraction effects, five cases of interest were compared for different values of porosity and Rayleigh number by means of averaged Nusselt number of hot and cold walls; and also local Nusselt number of enclosure walls. Comparison of different cases shows the geometrical dependence of overall heat transfer performance via the average Nusselt number of hot pins strongly depending on their position. The four pin case with diamond arrangement shows the best performance in the light of enclosure walls' average Nusselt number (heat transfer to cold walls). However, the case with three pins and downward triangular arrangement surprisingly gives promising heat transfer performance. In addition, the results show that natural convective heat transfer and flow field is intensified with increasing Rayleigh number, Darcy number, and porosity.

Keywords: Natural Convection; Pin-fins Configuration Effects; Porous Medium; Nanofluids; LBM.

NOMENCLATURE

c	lattice streaming speed
c_s	speed of sound
c_i	discrete lattice velocity
Da	darcy dumber ≡ K/L^2
F	total body force vector
F_i	discrete body force in LBM
f_i	density distribution function
f_i^{eq}	equilibrium density distribution Function
G	buoyancy force term per unit mass
g_i	internal energy distribution function
g_i^{eq}	equilibrium internal energy distribution Function
g_i^{neq}	non-equilibrium internal Energy distribution functions
g_0	acceleration due to gravity
K	permeability of porous media
L	height and width of the cavity
Nu	Nusselt number
Pr	Prandtl number
R	radius of curve boundary
Ra	Rayleigh number
T	temperature
U	fluid velocity vector
V	temporal velocity
x,y	cartesian coordinates

Greek Letters

E	porosity of the Media
A	thermal conductivity
B	thermal expansion coefficient

N	kinetic viscosity
τ_c	relaxation time for temperature
τ_v	relaxation time for flow
Θ	dimensionless temperature
P	fluid density
Φ	volume Fraction of Nanoparticles

Subscripts

c	cold
h	hot
nf	nanofluid
f	base fluid
s	solid Particles
ave	average
loc	local

1. INTRODUCTION

Nowadays, engineers are dealing with dissipating heat flux in porous media for many thermal applications, such as porous heat exchangers, electronic cooling systems, etc. As an economic heat transfer mechanism, natural convection is favorable for engineers because of its simple nature, while it saves energy substantially without making noise. On the other hand, having access to devices with smaller dimensions, lighter weight and more efficient heat transfer has resulted in investigation of related optimum designs. Although more surfaces lead to enhancement of natural convective heat transfer, this approach is not possible for all applications due to spatial limitation. Besides, using nanofluids is a practical technique to improve heat transfer. Hence, improvement of natural convective nanofluid heat transfer in porous media has been the focus of many investigations in recent decades (Clague and Phillips 1997; Nield and Bejan 1999; Hsu and Vafai 2005; Tomadakis and Robertson 2005).

Recently, LBM has been developed as an alternative and promising numerical scheme for fluid flow and heat transfer. Compared with classical computational fluid dynamics, lattice Boltzmann method is a meso-scale modeling method, based on the particle kinematics, which makes it very suitable for micro-scale simulations (Succi 2001; Sukop and Thorne 2006; Mohamad 2011). Nowadays, LBM has achieved great success in multiphase, chemical reacting, thermos-hydrodynamic, particle laden, and magneto-hydrodynamic flows. Recently, lattice Boltzmann simulation has showed its capabilities in prediction of fluid flow behavior in porous medium (Spaid and Phelan 1997, 1998; Dardis and McCloskey 1998; Freed 1998; Martys 2001; Kang *et al.* 2002). The representative elementary volume (REV) porous media models have been demonstrated to be relatively more efficient for modeling porous flows. However, they are based on semi-empirical models (based on the volume-averaging at the REV scale), which have been developed through many years (e.g., Darcy, Brinkman-extended Darcy, Forchheimer-extended Darcy, Brinkman and Forchheimer-extended Darcy models) (Hickox and Gartling 1985; Nishimura *et al.* 1986; Tien and Vafai 1989; Hsu and Cheng 1990; Gartling *et al.* 1996; Nithiarasu *et al.* 1997; Al-Amiri 2000). Recently, a generalized lattice Boltzmann equations (GLBE) has been proposed to overcome the drawbacks of Darcy, Brinkman, and Forchheimer models for incompressible flows (Guo and Zhao 2002). Also, Salimi et al. coupled LBM with finite volume method as a hybrid method to study heat transfer flows (Salimi *et al.* 2015a,b,c).

During the last decade, many LBM heat transfer studies were focused on natural convection in porous medium (Guo and Zhao 2005; Seta *et al.* 2006; Yan *et al.* 2006; Zhao *et al.* 2010; Jafari *et al.* 2015a,b,c). Guo and Zhao (2002) have suggested a lattice Boltzmann model for isothermal incompressible flow in porous media. They introduced source terms in the equilibrium distribution function to involve the linear and non-linear drag force effects. Later, they studied laminar convection of a fluid featuring temperature-dependent viscosity in porous medium (Guo and Zhao 2005). Seta *et al.* (2006) have evaluated the reliability and efficiency of lattice Boltzmann method for simulation of natural convection in porous media at the representative elementary volume scale (REV). The comparison of solutions between their model and earlier studies showed good quantitative agreements for the whole range of Darcy and Rayleigh numbers. Yan *et al.* (2006) numerically investigated the natural convective heat transfer in a square cavity, filled with a heterogeneous porous media, using LBM. They concluded that the porosity near the walls has significant influence on heat transfer, while the porosity in the middle of the cavity has negligible effects. Zhao *et al.* (2010) presented a thermal lattice Boltzmann model with dual distribution functions to simulate a two-dimensional natural convection flow in porous media (metal porosity).

Haghshenas *et al.* (2010) analyzed natural convection in an open-end square cavity via a new algorithm, using LBM. Varol (2012) has analyzed heat transfer and flow field between two entrapped porous trapezoidal cavities, involving cold inclined walls and hot horizontal walls. Besides, researchers have used LBM to study the effect of magnetic field on natural heat transfer in porous media (Hasanpour *et al.* 2012; Ashorynejad *et al.* 2012; Sheikholeslami *et al.* 2013a; Husseini *et al.* 2014; Servati *et al.* 2014). For instance, Servati *et al.* (2014) studied the effect of vertical magnetic field on the flow pattern for partially field porous media and reported the MHD effect on natural convection.

Simulation of nano-fluid flow, using LBM, has been interesting to many researchers in the past decade (e.g., Xuan and Yao 2005; Nemati *et al.*, 2010; Sheikholeslami *et al.*, 2013b; and Jafari *et al.* 2015). These researchers were mainly concentrated on heat transfer effects in different geometries (e.g., NorAzwadi 2014). More recently however, more complex problems, such as magnetic field effects, more complex geometries, mixed convection, etc. have been investigated (e.g., Karimipour, 2015; Rahmati, 2016;

Alsabery, 2017; and Arjun and Kumar 2017).

In this research, concerning the geometrical effects on natural heat transfer in porous media, different cases with various configurations were studied in regards to small scale of a cooling pin-fins system. A square enclosure is considered with hot inner fins (cylinders) in a porous media. Different cases were compared in order to study the effects of arrangement and number of fins on natural convective heat transfer in homogenous porous media. To model porous media, Brinkman-Forchheimer generalized equation was utilized. Lattice Boltzmann method with two distribution functions was solved for flow and temperature fields, while the effects of porous media were added to the equilibrium equations as source terms, including Brinkman-Forchheimer terms. Comparison for different conditions was conducted and average Nusselt numbers of hot and cold walls were reported. The best case was chosen to study controlling parameters, such as Rayleigh number, porosity factor, and Darcy number.

As follows, the problem studied is illustrated in details and different configurations are presented. Next, the numerical methodology is covered comprehensively, including governing equations, nanofluid relations, discretization, and boundary conditions. We aided to clarify all details of numerical simulation in order to provide a complete source for other thermal LBM researchers. Then, the independency of the solution to the grid was assumed. Besides, the results were evaluated by comparison with previous reported results. After proving our numerical simulation in all aspects, results for different configurations are presented and discussed from different viewpoints. Finally, the best case is investigated for different ranges of controlling parameters.

2. PROBLEM DESCRIPTION

Figure 1 illustrates the five cases studied in this work. A square cavity with side L was considered as the outer boundary, while cylinders with constant characteristic area played the role of hot surfaces. The ratio R/L was set 0.2 for the case of a single cylinder. Square cavity walls and inner cylinders' surfaces were fixed at constant cold (T_c) and warm (T_h) temperatures, respectively. The space between the cavity and the cylinders was a porous medium. Water-copper nanofluid and air were utilized as working fluids for simulation and validation, respectively. Thermo-physical properties of operating these fluids are listed in Table 1 (Abu-Nada *et al.* 2008). The inner cylinder's arrangement of one, three (two modes), and four cylinders (two modes) were studied thoroughly. The radius of the inner cylinders was determined in such a way that the total heat transfer surface was fixed in all five cases. Note, in this two-dimensional study, the magnitude of this surface is proportional to the cylinder's perimeter. The coordinates of the center of cylinders in the inner three-cylinder arrangements coincide with vertices of an equilateral triangle inscribed in a single cylinder, while the ones for the inner four-cylinder arrangements coincide with vertices of a square inscribed in a single cylinder.

As the main objective of this study, this work aims to find the best configuration in light of the numbers and the arrangement of cylinders in order to have the best heat transfer performance in porous medium. Moreover, the influence of the porous medium on the flow field and heat transfer characteristics of nanofluids natural convection is discussed completely. The effect of controlling parameters are investigated, using non-dimensional numbers, such as Rayleigh, Darcy, porosity, Nusselt, and volume fraction of nanoparticles on the flow field and heat transfer. In this study, we aim to give perception on geometrical effects of cooling pin-fins configuration in porous medium.

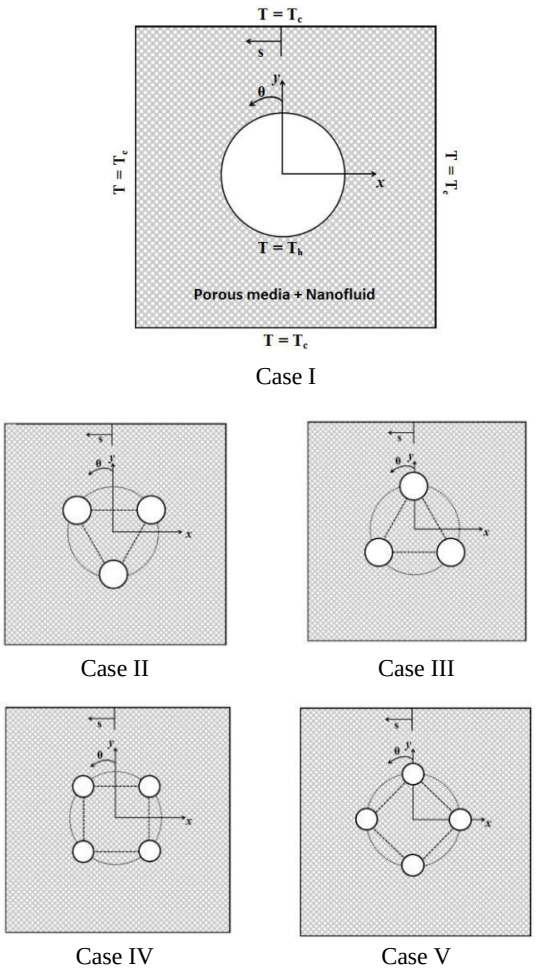

Fig. 1. Five different cases considered.

3. SOLUTION OF THE PROBLEM

In this study, natural convection in porous media was simulated, using Brinkman-Forchheimer equation and lattice Boltzmann method. As follows, numerical methodology and applied boundary conditions are described in details.

Table 1 Thermo-physical properties (Abu-Nada *et al.* 2008)

		Pr	ρ (kg/m^3)	C_p (J/kg.K)	K (W/m.K)	$\beta\times10^{-5}$ (K^{-1})	$\alpha\times10^{-5}$ (m^2/s)
Base Fluids	Air	0.7	1.2	1006	0.026	340	
	Water	6.2	997.1	4179	0.613	21	
Nano-particles	Copper (Cu)		8933	385	401	1.67	11.7

3.1 LBM Modeling in Porous Medium

The flow is assumed incompressible, while thermal equilibrium condition is used assumed in the porous medium. Based on these assumptions, continuity, momentum (with Brinkman-Forchheimer source terms), and energy equations can be expressed as Eqs. (1)-(3) (Seta *et al.* 2006).

$$\nabla.u = 0 \tag{1}$$

$$\partial_t u + (u.\nabla)(\frac{u}{\varepsilon}) = -\frac{1}{\rho}\nabla(\varepsilon P) + \nu_e\nabla^2 u + F \tag{2}$$

$$\frac{\partial T}{\partial t} + \nabla.(uT) = \alpha\nabla^2 T \tag{3}$$

In these equations, ε, ν_e and α are porosity, effective kinematic viscosity and thermal diffusivity, respectively. F encompasses viscous diffusion, inertia due to the presence of a porous medium, and buoyancy. As widely used, Ergun's relation below represents this body force, as:

$$F = -\frac{\nu\varepsilon}{K}u - \frac{1.75}{\sqrt{150\varepsilon K}}|u|u + \varepsilon G, \tag{4}$$

in which, ν, K and G are kinematic viscosity, permeability, and buoyancy force, respectively. The buoyancy force is calculated based on Boussinesq approximation, as $G = \beta g_0 \theta$.

In recent years, LBM has become a powerful technique in computational fluid dynamics and is based on overcoming the drawbacks of Lattice Gas Cellular Automata (LGCA). Flow and thermal fields are computed using two coupled distribution functions. The effects of porous medium appear in the distribution function of the flow field as a source term. There, standard D2Q9 lattice (Fig. 2a) is considered for both distribution functions. Note, f represents the flow field distribution function, which is (Bhatnagar *et al.* 1954; He *et al.* 1998; NorAzwadi, and Tanahashi 2006):

$$f_i(x + c_i\Delta t, t + \Delta t) = f_i(x,t) + \frac{\Delta t}{\tau_\nu}\left[f_i^{eq}(x,t) - f_i(x,t)\right] + \Delta t c_i F_i. \tag{5}$$

In addition, g indicates temperature field distribution function as (Bhatnagar *et al.* 1954; He *et al.* 1998; NorAzwadi, and Tanahashi 2006):

$$g_i(x + c_i\Delta t, t + \Delta t) = g_i(x,t) + \frac{\Delta t}{\tau_c}\left[g_i^{eq}(x,t) - g_i(x,t)\right] \tag{6}$$

Where, Δt, c_i and F_i represent lattice time step, discrete speed in ith direction, and body force, respectively. Also, τ_v and τ_c indicate relaxation time for flow and temperature fields, respectively. Equation (5) recovers continuity and momentum conservation (Eqs. (1) and (2)), while Eq. (6) describes the conservation of internal energy (Eq. (3)). The fluid macroscopic quantities, such as density and temperature, are defined as $\rho = \Sigma_i f_i$ and $T = \Sigma_i g_i$, respectively. The fluid velocity (**u**) is calculated using a temporal velocity (**V**) to consider the effects of porous media. Note, **u** and **V** are defined as follows (Yan *et al.* 2006):

$$u = \frac{V}{c_0 + \sqrt{c_0^2 + c_1|V|}}, \tag{7}$$

$$V = \sum_i \frac{c_i f_i}{\rho} + \frac{\varepsilon G}{2}, \tag{8}$$

$$c_0 = \frac{1}{2}(1 + \varepsilon\frac{\nu}{2K}), \tag{9}$$

$$c_1 = \varepsilon\frac{1.75}{2\sqrt{150\varepsilon^3 K}}. \tag{10}$$

Considering porous medium, equilibrium distribution function (f_i^{eq}) is defined as (Bhatnagar *et al.* 1954; He *et al.* 1998; NorAzwadi, and Tanahashi 2006):

$$f_i^{eq} = \omega_i\left[1 + \frac{c_i.u}{c_s^2} + \frac{1}{2}\frac{(c_i.u)^2}{\varepsilon c_s^4} - \frac{u^2}{2\varepsilon c_s^2}\right]. \tag{11}$$

Similarly, the equilibrium distribution function for thermal distribution (g_i^{eq}) is (He *et al.* 1998; NorAzwadi, and Tanahashi 2006):

$$g_i^{eq} = \omega_i T\left[1 + \frac{c_i.u}{c_s^2}\right], \tag{12}$$

Where, ω_i is the weighting factors. c_s shows the sound speed, which is equal to $c_s = c/\sqrt{3}$, where *c* is the lattice spacing. For D2Q9, discrete speeds and weighting factors are defined as (Mohamad 2011):

$$c_0 = 0,$$

$$c_i = c(\cos(\frac{(i-1)\pi}{2}), \sin(\frac{(i-1)\pi}{2})), i = 1-4$$

$$c_i = \sqrt{2}c(\cos(\frac{(i-5)\pi}{2} - \frac{\pi}{4}), \sin(\frac{(i-1)\pi}{2} - \frac{\pi}{4})), \quad i = 5-8 \tag{13}$$

$$c_i = \begin{cases} 4/9 & i = 0, \\ 1/9 & i = 1,2,3,4, \\ 1/36 & i = 5,6,7,8. \end{cases} \quad (14)$$

(a)

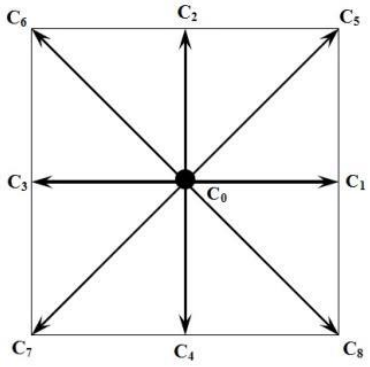

(b)

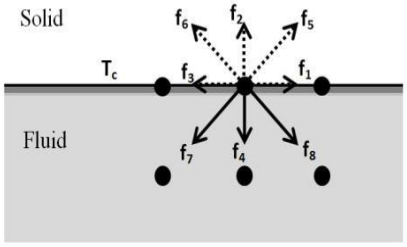

(c)

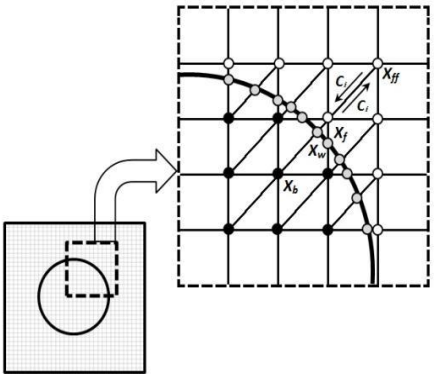

Fig. 2. (a) D2Q9 Discretization model (two-dimensional nine-velocity); (b) Bounce back technique for upper wall cavity; (c) Lattice nodes for curved boundary.

The body force (F_i) is defined (Salimi *et al.* 2015b):

$$F_i = \omega_i \rho (1 - \frac{1}{2\tau_v})[\frac{3c_i.F}{c^2} + \frac{9(uF : c_i c_i)}{\varepsilon c^4} - \frac{3u.F}{\varepsilon c^2}]. \quad (15)$$

In addition, ν and α are obtained by using following relations (Abu-Nada *et al.* 2008; Husseini *et al.* 2014; Servati *et al.* 2014):

$$\nu = (\tau_\nu - \frac{1}{2})c_s^2, \alpha = (\tau_c - \frac{1}{2})c_s^2. \quad (16)$$

Note, viscosity and thermal diffusion are always positive and thus both relaxation times should be greater than 0.5 (Mohamad 2011).

Boussinesq approximation has been used for modeling the buoyancy force due to natural convection. For stability purposes, the characteristic velocity of the flow due to the natural regime ($V_{natural} = (\beta g_y \Delta TL)^{0.5}$) must be small compared to the fluid speed of sound (Hickox and Gartling 1985). In the present study, the characteristic velocity was selected to be 10 percent of the sound speed.

Using the following dimensionless quantities:

$$X = \frac{x}{L}, Y = \frac{y}{L}, U = \frac{uL}{\upsilon}, V = \frac{\upsilon L}{\nu}, \quad \theta = \frac{T - T_c}{T_h - T_c}, \quad (17)$$

the dimensionless numbers, such as Rayleigh, Darcy, and local and average Nusselt number show their importance in our problem (Eqs. (18)-(21)):

$$Ra = \frac{\beta g_y L^3 (T_h - T_c)}{\nu \alpha} \quad (18)$$

$$Da = \frac{K}{L^3} \quad (19)$$

$$Nu_{loc} = \frac{k_{nf}}{k_f} \frac{\partial T}{\partial r} \quad (20)$$

$$Nu_{ave} = \frac{1}{L} \int_0^L Nu_{loc} dy \quad (21)$$

3.2 Nanofluids Relations

Thermal equilibrium and no-slip condition between the particles and the fluid are assumed. Note, the nanofluid is treated similar to a pure fluid, but with properties (e.g., density, heat capacity, and volume expansion coefficient) as (Khanafer *et al.* 2003; Wang and Mujumdar 2007):

$$\rho_{nf} = (1-\varphi)\rho_f + \varphi\rho_s, \quad (22)$$

$$(\rho c_p)_{nf} = (1-\varphi)(\rho c_p)_f + \varphi(\rho c_p)_s, \quad (23)$$

$$(\rho\beta)_{nf} = (1-\varphi)(\rho\beta)_f + \varphi(\rho\beta)_s, \quad (24)$$

Where, φ is the volume fraction of nanoparticles and subscripts f, s and nf indicate base fluid, nanoparticles, and nanofluid, respectively. The viscosity of nanofluid consisting of small suspended spherical particles is calculated through Brinkman relation (Brinkman 1952; Hwang *et al.* 2007), as:

$$\mu_{eff} = \frac{\mu_f}{(1-\varphi)^{2.5}}. \quad (25)$$

In order to calculate the thermal conductivity of nanofluid, several relations are introduced. In this study, due to low volume fraction, spherical, and identical nanoparticles and particles, thermal conductivity is computed using Maxwell approximation (Hwang *et al.* 2007), as:

$$\frac{k_{nf}}{k_f}=\frac{k_s+2k_f-2\varphi(k_f-k_s)}{k_s+2k_f-\varphi(k_f-k_s)}. \quad (26)$$

3.3 LBM Boundary Conditions

In order to model the solid boundary conditions to set non-slip flow around obstacles, the bounce back technique (Mohamad 2011) is used. For implementation of this technique, the unknown density distribution functions on the upper wall cavity (Fig. 2b) can be determined as follows:

$$\begin{aligned} f_4 &= f_2,\\ f_7 &= f_5,\\ f_8 &= f_6. \end{aligned} \quad (27)$$

First, to determine the thermal distribution function, the boundary conditions are set to match the constant temperature on the wall (Mohamad 2011). Therefore, the wall temperature is fixed (fixed value condition) on the upper wall by using the following relations:

$$\begin{aligned} g_4 &= \omega_4 T_c+\omega_2 T_c-g_2,\\ g_7 &= \omega_7 T_c+\omega_5 T_c-g_5,\\ g_8 &= \omega_8 T_c+\omega_6 T_c-g_6, \end{aligned} \quad (28)$$

Note, for the case of curved boundary, we have a totally different scenario. Generally, curved boundary implementation is relatively more complicated. This complexity comes from Cartesian nature of LBM, which causes the discrepancy between the exact location of the curved boundary and its grid points. Therefore, researchers have used a combination of mathematical and geometric relations (besides numerical techniques) to obtain acceptable methods with reasonable accuracy.

In this research, a curved boundary condition of second order accurate is utilized for the bounce back and fixed value conditions. The adjacent lattice nodes of curved boundaries are known as boundary nodes and are specified by subscript *b*. Distribution functions at the boundary nodes should be determined in such a way that the required condition on the boundary is satisfied (Fig. 2c).

In Fig. 2(c), the black points on a solid area represent the boundary nodes (x_b), while white points indicate fluid nodes (x_f). Considering the second point in the fluid (x_{ff}) leads to second order accuracy of boundary condition. Besides, the gray points (x_w) show the intersection of the boundary and the lattice edges in D2Q9. Finally, the macroscopic properties at the boundary are extrapolated using these nodes. The fraction of an intersected link (Δ) should be $0 \le \Delta \le 1$ and is described as:

$$\Delta=\frac{|x_f-x_w|}{|x_f-x_b|}. \quad (29)$$

After the streaming step, the distribution function at the boundary point xb needs to be calculated, using the fraction length Δ. There are different relations for the computation of distribution functions for the flow and temperature filed.

For the flow distribution function, curved boundary method proposed by Mei *et al*. (1999) has been used. They derived a second-order accurate boundary condition for a curved boundary. Their method is an improvement of the one introduced by Filippova and Hänel (1998).

In order to construct the post-collision distribution function, $\tilde{f}_{\bar{\alpha}}(x_b,t)$ based upon the known information of the neighboring lattices, a Chapman–Enskog expansion for the post-collision distribution function was used, as:

$$\begin{aligned} \tilde{f}_{\bar{\alpha}}(x_b,t) &= (1-\chi)\tilde{f}_{\alpha}(x_f,t)+\chi f^{*}_{\alpha}(x_b,t)\\ &+2\omega_\alpha\rho\frac{3}{c^2}e_{\bar{\alpha}}.u_w, \end{aligned} \quad (30)$$

Specifically, the distribution function, $f^{*}_{\alpha}(x_b,t)$, was defined as:

$$\begin{aligned} f^{*}_{\alpha}(x_b,t) &= f^{EQ}_{\alpha}(x_f,t)+\\ &+\omega_\alpha\rho(x_f,t)\frac{3}{c^2}e_{\bar{\alpha}}.(u_{bf}-u_f), \end{aligned} \quad (31)$$

$$\begin{aligned} &\chi=\frac{(2\Delta-1)}{\tau-2}\\ &u_{bf}=u_{ff}=u(x_{ff},t), \end{aligned} \qquad 0\le\Delta\le\frac{1}{2},$$

$$\begin{aligned} &\chi=\frac{(2\Delta-1)}{\tau-1/2},\\ &u_{bf}=\frac{1}{2\Delta}(2\Delta-3)u_f+\frac{3}{2\Delta}u_w, \end{aligned} \qquad \frac{1}{2}\le\Delta\le 1, \quad (32)$$

in which $e_{\alpha^-}=-e_\alpha$; $x_{ff}\equiv x_f+e_{\alpha^-}\delta t$; $u_f\equiv u(x_f,t)$ is the fluid velocity near the wall; $u_w\equiv u(x_w,t)$ is the velocity of solid wall; u_{bf} is imaginary velocity, and χ is a weighting factor depending on Δ.

Using the scheme of Yan *et al*. (2008), the temperature non-equilibrium distribution function could be calculated at boundary points, as:

$$g^{NEQ}_{\bar{\alpha}}(x_b,t)=g_{\bar{\alpha}}(x_b,t)+g^{EQ}_{\bar{\alpha}}(x_b,t). \quad (33)$$

While, Eq. (6) is replaced by Eq. (34) at boundary points for the streaming step, as:

$$\begin{aligned} \tilde{g}_{\bar{\alpha}}(x_b,t) &= g_{\bar{\alpha}}(x_b,t)\\ &-\frac{1}{\tau_c}[g_{\bar{\alpha}}(x_b,t)-g^{EQ}_{\bar{\alpha}}(x_b,t)]. \end{aligned} \quad (34)$$

Substituting Eq. (33) into Eq. (34), we obtain the thermal distribution function, as:

$$\tilde{g}_{\bar{\alpha}}(x_b,t)=g^{EQ}_{\bar{\alpha}}(x_b,t)+(1-\frac{1}{\tau_c})g^{NEQ}_{\bar{\alpha}}(x_b,t). \quad (35)$$

Obviously, the values of $g^{NEQ}_{\bar{\alpha}}$ and $g^{EQ}_{\bar{\alpha}}$ need to be

known in order to calculate $\tilde{g}_{\bar{\alpha}}$. According to Yan *et al.* (2008), the equilibrium value of $g_{\bar{\alpha}}^{EQ}$ is computed from the following equation:

$$g_{\bar{\alpha}}^{EQ}(x_b,t) = \omega_{\bar{\alpha}} T_b^* (1 + \frac{3}{c^2} e_{\bar{\alpha}} . u_b^*), \tag{36}$$

where, u_b^* is defined as:

$$\begin{aligned} u_b^* &= u_{b1}, && \Delta \geq 0.75, \\ u_b^* &= u_{b1} + (1-\Delta) u_{b2}, && \Delta \leq 0.75, \end{aligned} \tag{37}$$

$$\begin{aligned} u_{b1} &= [u_w + (\Delta - 1) u_f] / \Delta, \\ u_{b2} &= [2u_w + (\Delta - 1) u_{ff}] / (1 + \Delta), , \end{aligned} \tag{38}$$

and T_b^* is defined as:

$$\begin{aligned} T_b^* &= T_{b1}, && \Delta \geq 0.75, \\ T_b^* &= T_{b1} + (1-\Delta) T_{b2}, && \Delta \leq 0.75, \end{aligned} \tag{39}$$

$$\begin{aligned} T_{b1} &= [T_w + (\Delta - 1) T_f] / \Delta, , \\ T_{b2} &= [2T_w + (\Delta - 1) T_{ff}] / (1 + \Delta). \end{aligned} \tag{40}$$

To estimate the non-equilibrium distribution function at a boundary point (on solid boundary), the following conditions are used:

$$\begin{aligned} g_{\bar{\alpha}}^{NEQ}(x_b,t) &= g_{\alpha}^{NEQ}(x_b,t), && \Delta \geq 0.75, \\ g_{\bar{\alpha}}^{NEQ}(x_b,t) &= \Delta g_{\alpha}^{NEQ}(x_f,t) + && \\ (1-\Delta) g_{\alpha}^{NEQ}(x_{ff},t), && \Delta \leq 0.75. \end{aligned} \tag{41}$$

3.4 Independence Solution of Grid

To be assured of grid independency, different grid resolutions were studied for all different cases. For this investigation, all controlling parameters, such as Rayleigh number, Darcy number, porosity, and the volume fraction of particles were considered. Different grid cases were compared to the average Nusselt number of cold wall and the inner hot cylinder for the natural convection of nanofluids with 5% volume fraction in porous media with porosity of 0.01, Darcy number of 0.4, and Rayleigh number of 2e5. Although only the average Nusselt number of one cylinder of each case is plotted in Fig. 3, all the inner cylinders of the case shows same behavior. Besides, the average Nusselt number of the cold wall did not change for different grid numbers. All five configurations were studied for grids 140 × 140, 160 × 160, 180 × 180, 200 × 200, and 220 × 220. For all geometries, 180 × 180 grid appeared to be the optimal choice.

3.5 Code Validation

In order to validate our numerical simulation, three creditable works were used related to natural convection, porous media and curved boundary solution. In this way performance of our home-made code was evaluated for natural convective simulation for nanofluids. Initially, the work of Khanafer *et al.* (2003) was used in order to evaluate the accuracy of our simulation in sake of natural convection simulation of nanofluids (Fig. 4). Khanafer *et al.* (2003) have studied thermal performance for a two-dimensional enclosure, utilizing water–cu nanofluid. They reported data for Grashof numbers (Gr) 10^3<Gr<10^5, while their volume fraction (φ) varied as 0 %< φ<25%. The average Nusselt number of hot wall was measured for two Grashof numbers of 104 and 105 at various volume fractions of Nano particles. This comparison (Fig. 4) demonstrated good agreements between the present study and Khanafer results, particularly for volume fractions lower than about 6%, which error is trivial.

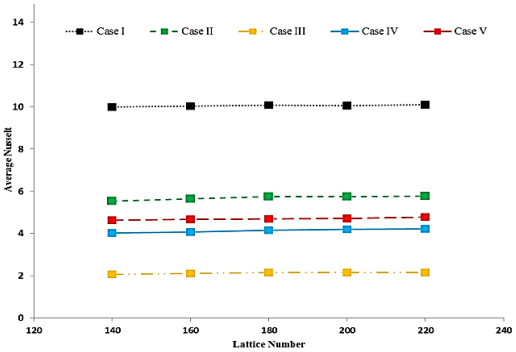

Fig. 3. Grid-independence for different geometries.

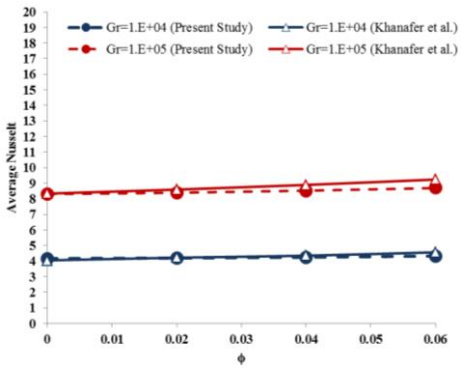

Fig. 4. Comparison of the average Nusselt number between the present study and the numerical results by Khanafer *et al.* (2003).

In order to validate the performance of our solver for porous media simulation, two credential works of Seta *et al.* (2006) and Nithiarasu *et al.* (1997) were used (Fig. 5). The average Nusselt number of the cold outer cavity walls was compared for different three porosity of 0.4, 0.6, and 0.9 at three different Rayleigh numbers. In this simulation, the horizontal cavity walls were assumed to be insulated and the left and right vertical walls were kept at different temperatures. Comparative results indicate excellent performance of the present solution and assure the following results for natural convection in porous media. The maximum error was 2.2%, which demonstrates a decent performance of our home-made code.

Since the curved boundary condition could initiate

serious inaccuracy, we used a credible source to validate our curved boundary implementation. Thus, the results of Moukalled and Acharya (1996) for average Nusselt number of curved heated wall were repeated, using our code. Moukalled and Acharya studied natural convective heat transfer in a heated coaxial cylinder in square cavity with R/L = 0.1, 0.2, and 0.3 and four different Rayleigh numbers: Ra = 10^4, 10^5, 10^6, and 10^7. Three Rayleigh numbers (10^4, 10^5 and 10^6) at different curve radius inner cylinder were simulated and compared to the reported results in Fig. 6. According to the results, the maximum error of 6% indicates sufficient performance of our code for curved walls.

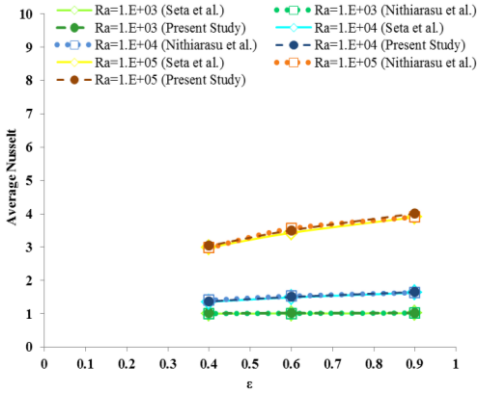

Fig. 5. Comparison of the average Nusselt number between the present study and the numerical results by Seta *et al.* (2006) and Nithiarasu *et al.* (1997).

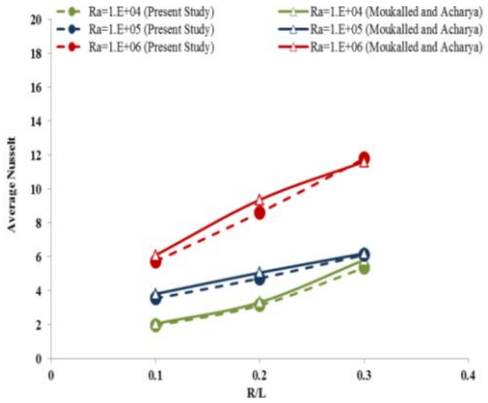

Fig. 6. Comparison of the average Nusselt number between the present study and the numerical results by Moukalled and Acharya (1996).

4. RESULTS AND DISCUSSION

After validation and verification of our home-made code, the natural convection of nanofluids in a porous medium was studied for the described configurations. As the prime aim of this study, the effect of hot cylinders numbers and arrangements, volume fraction of nanoparticles, and non-dimensional parameters, such as Rayleigh and Darcy numbers, and porosity were investigated, in order to decide about the best case for natural convective heat transfer performance. Our LBM simulation started from an initial equilibrium state with constant density $\rho = 1$. The normalized velocity and temperature were initially set to zero and 0.5, respectively. After validating the numerical code developed in the present investigation, it was used to carry out a number of simulations for a range of controlling parameters. The range of Rayleigh numbers for this investigation varied from 10^4 to 10^6, the Darcy number ranged between 10^{-2} and 10^{-4}, and porosity varied from 0.4 to 0.9. Moreover, the effect of nano-particles was studied by volume fraction φ variation between 0 and 0.05.

Initially, in order to study the effect of nanoparticles, water based nanofluids, containing various volume fractions of Cu nanoparticles were utilized. Simulation of various volume fractions of nanoparticles was conducted for a cavity with hot inner cylinder (Case I) considering different Rayleigh numbers at ε=0.4 and Darcy number of 0.01 (Fig. 7). The comparison concerns the average Nusselt number of the hot inner cylinder and the cold outer cavity. The average Nusselt number rises almost linearly by increase of nanoparticles for various Rayleigh numbers. The presence of nanoparticles in fluid enhances Nusselt number by about 15% for Ra= 10^4, Ra= 10^5 and Ra= 10^6 at volume fraction of φ=0.05. Besides, the average Nusselt number substantially increases for augmentation of Rayleigh number for constant nanoparticle volume fraction. In fact, this order of enhancement in the average Nusselt number can be significant for cooling applications, such as in electronic systems.

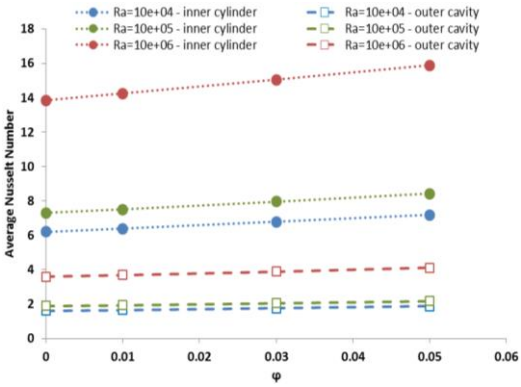

Fig. 7. Effect of nanoparticle volume fraction on average Nusselt number for various Rayleigh numbers (Case I).

Concerning local heat transfer, Fig. 8 shows the effect of nanoparticles on local Nusselt number of the hot inner cylinder, the outer cold walls and the velocity profiles at the central line (y=0.5) for nanofluid water-cu, while Rayleigh number and porosity are fixed at Ra=10^5, ε=0.4, and Darcy number is 0.01. Figure 8(a) shows that higher volume fraction increases the random motion of particles and leads to higher energy transfer rates in the fluid. Therefore, velocity profile takes higher peaks for higher volume fraction. Also, increasing volume fraction significantly increases the local

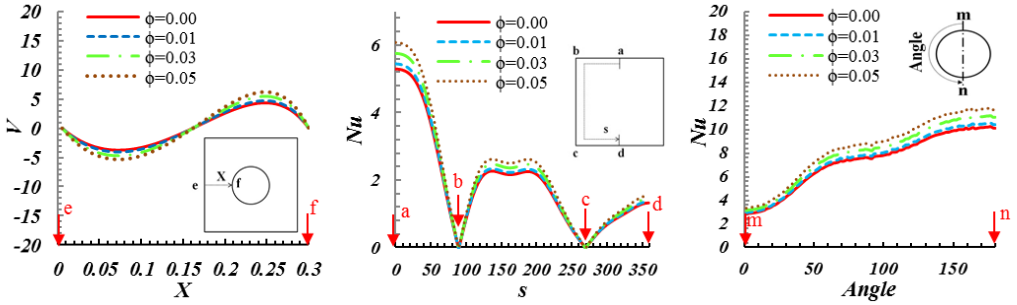

(a) (b) (c)

Fig. 8. Effect of nanoparticle volume fraction on (a) velocity profile, (b) local Nusselt number of the outer wall and (c) local Nusselt number of the inner cylinder, Ra=10^5 ε=0.4 and Da=0.01 (Case I).

Table 2 Average Nusselt number for inner hot cylinder at Da= 0.01

		Ra	10^4			10^5		
		ε	0.4	0.6	0.9	0.4	0.6	0.9
Case I	Inner Cylinder		7.1728	7.1894	7.2203	8.4100	9.1866	10.1595
Case II	Upper Left Cylinder		2.2021	2.1710	2.1486	2.6091	2.8034	3.0115
	Upper Right Cylinder		2.2197	2.1892	2.1674	2.6242	2.8113	3.2026
	Lower Cylinder		2.7726	2.9234	3.1088	4.8654	5.3266	5.7940
Case III	Lower Left Cylinder		2.5530	2.6407	2.7541	4.0354	4.4211	4.8336
	Lower Right Cylinder		2.5686	2.6559	2.7687	4.0411	4.4216	4.8286
	Upper Cylinder		2.0410	1.9348	1.8173	1.7263	1.9031	2.1003
Case IV	Lower Left Cylinder		1.9458	2.0463	2.1731	3.4664	3.8270	4.1857
	Lower Right Cylinder		1.9393	2.0406	2.1684	3.4712	3.8341	4.1932
	Upper Left Cylinder		1.4928	1.4334	1.3730	1.4479	1.5766	1.7316
	Upper Right Cylinder		1.4807	1.4201	1.3585	1.4431	1.5681	1.7289
Case V	Right Cylinder		1.7337	1.7589	1.7997	2.4613	2.6955	2.9417
	Left Cylinder		1.7495	1.7747	1.8152	2.4705	2.6998	2.9407
	Lower Cylinder		2.0761	2.2149	2.3859	3.9549	4.3659	4.7751
	Upper Cylinder		1.3858	1.2799	1.1637	1.1344	1.3132	1.5069

Nusselt number of the cold and the hot walls (Figs. 8 b and c) as is predicted by others (Khanafer *et al.* 2003). Note, nanofluid with 5% volume fraction substantially boosts up heat transfer rate. Thus, water-copper nanofluid with volume fraction of 5% is chosen to compare different cases.

As described before, five cases with different inner cylinder configurations were considered to find the optimal geometry in sake of natural convection in porous medium. Note, heat transfer can be examined from two aspects; first heat transfer from inner hot cylinder(s) and second heat transfer to the outer cold walls. Due to various inner cylinder numbers and configurations, comparison of the cases does not appear to be applicable for the first aspect. However, comparison in matter of heat transfer to the cold walls is reasonable and applicable from engineering point of view. Thermal and flow fields of each configuration are illustrated here using temperature and velocity contours. Moreover, the average Nusselt number of the inner hot cylinders and the outer cold walls are presented in Tables 2 and 3, respectively, in order to decide about the heat transfer performance of each configuration.

To understand, using the flow and thermal fields for each case, Fig. 9 demonstrates the geometrical effects, using streamlines and temperature contours at Ra=10^5 and 10^4, Da=0.01, and ε=0.4. According to these results, the flow is formed solely by natural convective thermal motion (Figs. 9). For all cases studies, streamlines and temperature contours show symmetric patterns about the central vertical line. The results show that the flow generally moves radially outward along the vertical symmetry line towards the cavity top cold wall (Figs. 9).The flow pattern and vortex locations strongly depend on the cylinders' configurations. It is also precisely shown that heat transfer is intensified and streamlines are more squeezed and distorted (particularly in the middle space between hot walls) for higher number of cylinders. For low Rayleigh number (e.g. Ra=10^4), the isotherms are more pronounced since the conduction heat transfer is still significant compared to developing natural convection. The upward natural convective flow is weak and the

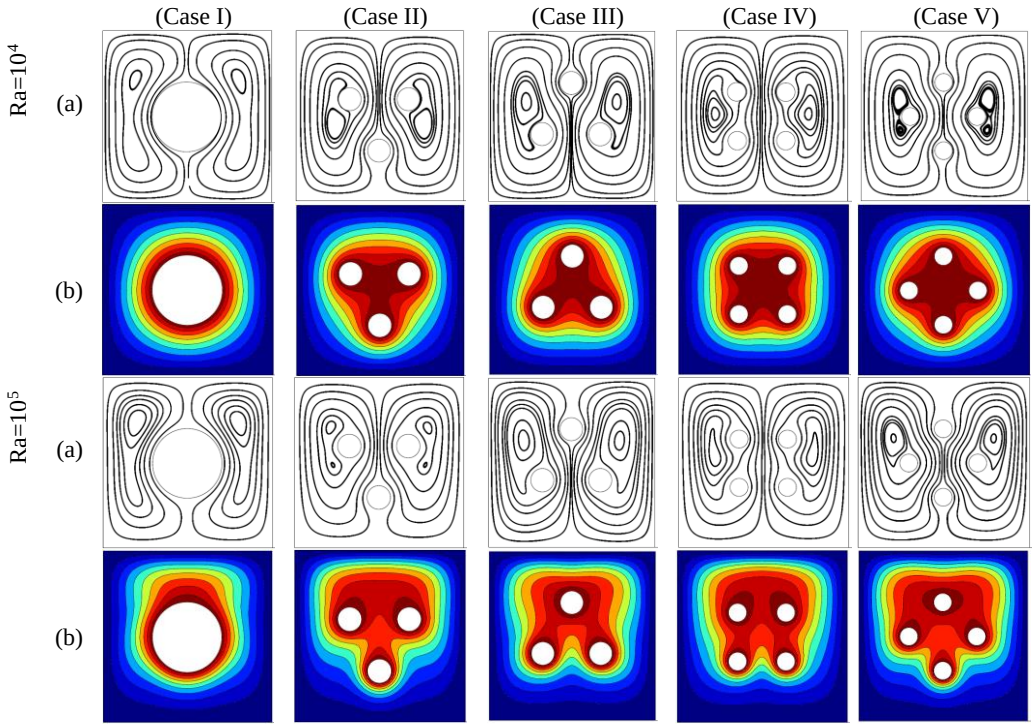

Fig. 9. (a) Streamlines and (b) temperature contours of different cases studied for ε=0.4 and Da=0.01.

thermal field is governed by conduction mechanism. However, the intensified convection (opposite to gravity direction) expands for high Rayleigh number (e.g. $R=10^5$) and pushes up the streamlines and isotherms. This change of heat transfer mechanism is considerable when Rayleigh number increases and the slightly squeezed twisted isotherms move upward. The dominant convective flow changes heat transfer pattern substantially. For high Rayleigh number, the middle space between cylinders faces lower temperature, whereas the central area was dominant by high temperature for low Rayleigh number. As the Rayleigh number increases from 10^4 to 10^5, the isotherms move upward, indicating higher local heat transfer rate to the upper cold walls. Also, streamlines are stretched towards the cold walls, while recirculation regions are pushed upward. The streamlines show relatively higher velocities for middle and top regions of enclosure, which is boosted for higher Rayleigh numbers.

Comparing different configurations illustrates that flow pattern and vortex positions vary depending on the numbers and arrangement of internal cylinders. Generally, the flow field is intensified for multi-cylinder cases compared to the single-cylinder configuration. In the cases with four cylinders, the streamlines cover greater spaces. Generally, we have at least one recirculation region at each side within overall symmetric rotating region, while its strength and position varies for different configurations. Temperature contours show that temperature gradient changes according to the numbers and arrangements of the inner cylinders. As the cylinder gets closer to the top of the cavity, the temperature gradient around it will be less intensified, since it is under the effects of natural convective flow from lower cylinders. Lower cylinders face higher thermal gradients. Therefore, inner cylinders' numbers and arrangements substantially change the heat transfer behavior.

Although flow field and thermal contours show the effects of inner cylinders' configurations (for fixed heating surfaces) on natural convection, some quantitative heat transfer parameters different needs to be studied for compare cases. Tables 2 and 3 show the average Nusselt number of the inner hot cylinders and the outer cold wall, respectively. In Table 2, the average Nusselt numbers of inner cylinder(s) have been detailed for $Ra=10^4,10^5$, $\varepsilon=0.4, 0.6, 0.9$, and for Darcy number of 0.01 for different cases studied. For the single-cylinder case, the average Nusselt number of cylinder shows the effect of porosity and Rayleigh number. However, the average Nusselt number of the inner cylinders (cases II -V) strongly depends on their position. Generally, the upper cylinders are considerably under the effects of released heat from the lower cylinders. Therefore, the average Nusselt number of the upper cylinders decreases by the increase of Rayleigh number, whereas average Nusselt number increases for higher Rayleigh number, as is obvious for other cylinders.

Considering the porosity effects, it is interestingly noticeable that the average Nusselt number of the upper cylinders diminish for higher porosity, while the average Nusselt number of the lower cylinders boost up for smaller Rayleigh numbers (e.g., $Ra=10^4$). At higher Rayleigh numbers (e.g. $Ra=10^5$), the average Nusselt number of all the inner cylinders increase for various porosity values.

Table 3 Average Nusselt number for cold outer cavity at Da= 0.01

	Ra	10^4			10^5		
	ε	0.4	0.6	0.9	0.4	0.6	0.9
Case I		1.8658	1.8702	1.8782	2.1733	2.3744	2.6268
Case II		1.9627	1.9865	2.0244	2.7355	2.9644	3.2026
Case III		1.9558	1.9742	2.0034	2.6522	2.9081	3.1860
Case IV		1.9436	1.9663	2.0033	2.7584	3.0349	3.3261
Case V		1.9647	1.9876	2.0251	2.8153	3.1121	3.4210

The main reason for this is the buoyancy effect caused by lower cylinders on flow and temperature fields. In lower Rayleigh numbers, these exist less effects of lower cylinder(s) on upper cylinder(s), since the buoyancy force is relatively weaker. In fact, the average Nusselt number of the upper cylinder(s) raises for increasing porosity, while enhancement rate is not the same for lower cylinders. This is because; the upper cylinder(s) are under the effects of lower ones. Notice that there is a small amount of discrepancy (less than 1%) for Nusselt number of symmetry cylinders in Table 2 due to numerical errors.

The heat transfer of inner cylinders are also studied considering their configurations, using the average Nusselt of each cylinder, whereas we need another parameter to compare thermal performance of different cases. The measured average Nusselt number of outer cold walls are listed in Table 3 for $Ra=10^4$, 10^5, ε=0.4, 0.6, 0.9, and Darcy number of 0.01. According to the results, the average Nusselt number of outer walls substantially increases with either augmentation of porosity or Rayleigh number. We aim to find the optimal case for heat transfer to the cold walls. Comparing the results of all cases shows that the multi-cylinder cases (Case II, III, IV and V) lead to better heat transfer, while they have the same heating areas. The numbers and the arrangements of cylinders considerably affect thermal performance. In fact, case V with four cylinders and diamond arrangement shows the best heating performance, while the second best case depends on Rayleigh number. For $Ra=10^4$, the three cylinder case recorded better performance than cases IV. While, case II takes the second place. This observation proves that the arrangement of cylinders is as important as their numbers. In case IV, the position of upper cylinders is exactly on the top of the lower ones, which leads to the deficiency of upper cylinders. As a result, Case IV doesn't show acceptable performance. It is interesting to know that with three cylinders we could accomplish heating capability as good as which four cylinders. Besides, for $Ra=10^5$ case IV gives slightly higher Nusselt number than cases IV and II for the porosity range. In this Rayleigh number, case IV ranked second, while case II still closely compete with four cylinder cases. Consequently, heat transfer operation of inner hot cylinder(s) hardly depends on their numbers, arrangements and working condition. Considering manufacturing cost for cooling system engineers, having nearly same performance by means of lower pins is appreciable.

In order to locally study the heat transfer to outer cold walls, the local Nusselt number is plotted along half to the cavity walls (Fig. 10). Comparison is conducted for $Ra=10^5$, ε=0.4, and Darcy number of 0.01, while the local Nusselt is plotted for left half of the cavity. As noted from this figure, Case V leads to highest local Nusselt number, while Case I causes the lowest local Nusselt for most of the points, particularly the side walls. This result matches with the results contained Table 3. about the best configuration. It is noticeable in Fig. 9 that the maximum and minimum values of local Nusselt number occurred at midpoints and corners, respectively. The minimum value of zero Nusselt number represents the corners of outer cavity, where the flow is stagnate. Thus, stagnation of the flow leads to no thermal gradient around the existing vertices. In addition, the maximum value occurs at the sides of the cavity; however its exact location depends on the factors affecting the natural convection (such as Rayleigh number).

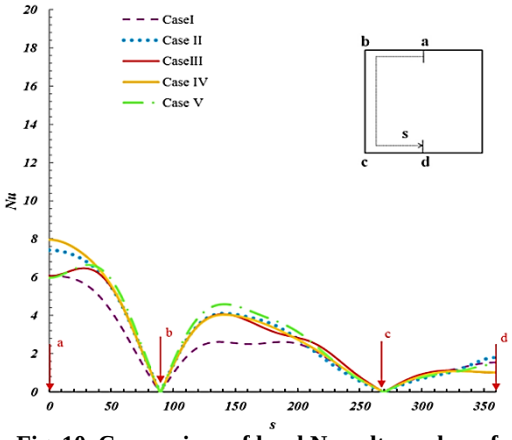

Fig. 10. Comparison of local Nusselt number of outer cavity in $Ra=10^5$, ε=0.4, and Darcy number of 0.01.

Concerning natural convective heat transfer, five cases were compared in light of local and average Nusselt number to find the optimal configuration and Case II surprisingly shows competitive result. It is even more interesting when fabrication cost comes into account. Having almost the same performance, with less cylinders, would be appealing for cooling system designers. However, purely theoretical analysis converges to case V, which shows the optimal performance for all tested parameters. Therefore, we choose the diamond four cylinders case (Case V) to study controlling factors (Rayleigh, Darcy and porosity) as follows.

In Fig. 11, Darcy number and porosity are fixed (ε=0.4 and Da=0.01) and the effect of Rayleigh

number on the local Nusselt number of cold wall and Velocity profile for Case V are plotted. Figure 11(a) shows the effect of Rayleigh number on vertical component of velocity at the horizontal centerline, passing the center. According to these diagrams, the amount of velocity profile increases (the same as the local Nusselt number) with increasing Rayleigh number. This higher velocity profile causes natural convection dominance in heat transfer mechanism. The presence of recirculation regions improves the convective flow substantially, when Rayleigh number gets higher.

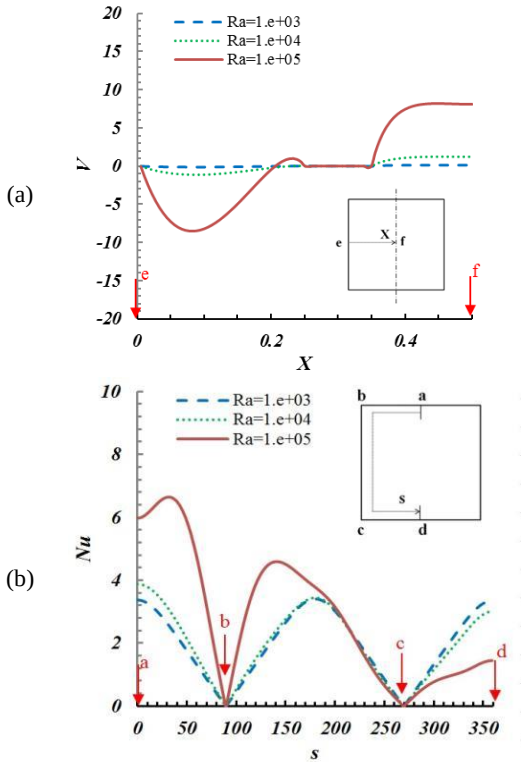

Fig. 11. Rayleigh number effects for Case V at ε=0.4 and Da=0.01 on (a) vertical component of velocity (b) local Nusselt number of the outer cavity

Figure 11(b) shows the effect of Rayleigh number on local Nusselt number of the outer cavity. According to the results, the local Nusselt number of top and side walls increases remarkably, although lower edge shows diminished local Nusselt value. For low Rayleigh number, (e.g. $Ra=10^3$), the Nusselt number profile is nearly symmetrical, while conduction heat transfer mechanism is still significant and leads to considerable heat transfer from the bottom of the cavity at $c \le s \le d$. Significant increase in heat transfer due to higher Rayleigh number is observed particularly at the top surface of the cavity because of developing convective heat transfer at the top of the cylinders. In fact, augmentation of Rayleigh numbers leads to denser isotherm lines at upper area which means the enhancement of local Nusselt number. Therefore, the Nusselt profile is no longer symmetrical while we have the local maximum Nusselt number at the top surface. The reason for this variation is the domination of conduction heat transfer by increasing Rayleigh number.

As discussed earlier using Tables 2 and 3, higher porosity increases the average Nusselt number of the outer walls. However, its effect on the inner cylinders hardly depends on cylinder's position. Also, since low porosity means more resistance to fluid flow, flow field is damped for low porosity values. Oppositely, isotherms become denser near the wall towards the upper half of the cavity and lower cylinder for higher porosity. This results in higher temperature gradient and consequently higher Nusselt number.

In order to locally examine the effect of porosity, velocity distribution and local Nusselt number of cold walls are shown for $Ra=10^5$ and Darcy number of 0.01 for case V (Fig. 12). Velocity profile matches with discussed contours in which lower resistance (by higher porosity) leads to higher natural convection. This is more pronounced for velocity profile of Fig. 12(a). The local Nusselt number of half of the outer cavity is plotted in Fig. 12(b). It is noticeable that higher porosity produces more convective heat transfer and as result higher thermal gradient at the upper walls. Whereas, the local Nusselt number for lower cold walls of cavity decreases with augmentation of porosity. Higher porosity lets the flow advance through the enclosure resulting in more dominant convective heat transfer. Thereupon, natural convection occurs better at higher porosity.

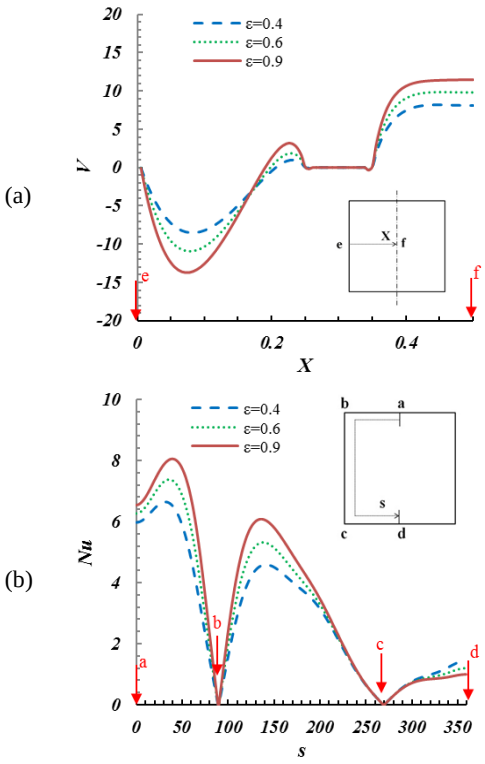

Fig. 12. Porosity effects for Case V on (a) vertical component of velocity and (b) on local Nusselt number of the outer cavity, at $Ra=10^5$and Da=0.0.1.

On the other hand, Darcy number is studied using temperature contours, streamlines, local velocity and local Nusselt number. Generally, for a given Rayleigh number and porosity, due to the higher permeability of the medium which results in increased velocity, the average Nusselt number increases with Darcy number. Figure 13 illustrates the Darcy number effects on streamline and temperature contours for Rayleigh $Ra=10^5$ and porosity $\varepsilon=0.4$. This figure shows that simulate to porosity, Darcy number increases convective flow. For Darcy number of 10^{-4}, porous medium doesn't allow natural convection to occur, while strong convective flow is developed for Darcy number of 10^{-2}. By increasing Darcy number, flow vortices are moved upward and thermal field migrates towards the top surface due to convection heat transfer dominance.

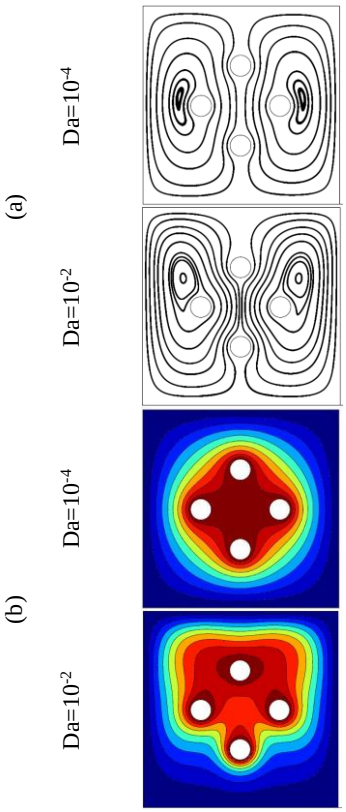

Fig. 13. Darcy number effects for Case V on; (a) streamlines and (b) temperature contours at $\varepsilon=0.4$ and $Ra=10^5$.

Besides, Darcy number effect is studied locally using the velocity profile (Fig. 14.a) and local Nusselt of the cold walls (Fig. 14.b). As observed in Fig. 13, the flow recirculation region located adjacent to the side cylinders. For higher Darcy number flow, circulation is intensified, which develops more convective heat transfer. The enhanced convective flow leads to higher Nusselt number of the upper walls in Fig. 14(b). Nearly symmetric plot of local Nusselt number for Darcy number 10^{-4}, which means equal heating of all cold walls, turned into an inclined diagram, indicating high heat transfer into the upper walls.

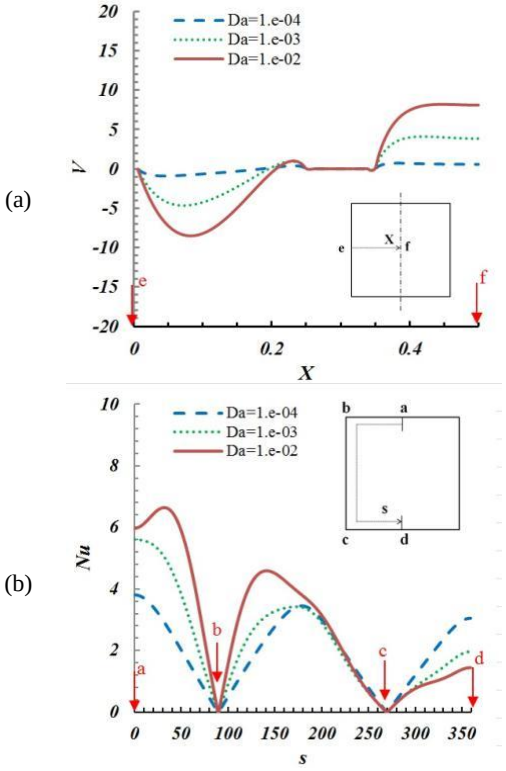

Fig. 14: Darcy number effects for Case V at $\varepsilon=0.4$ and $Ra=10^5$ on (a) vertical component of velocity and (b) local Nusselt number of the outer cavity.

5. CONCLUSION

In this study, flow and heat transfer of a nanofluid's natural convection between a cold square enclosure and warm inner cylinder(s) (via different inner cylindrical pin-fins configurations) field with homogeneous porous media were simulated, using a FORTRAN LBM homemade computer code. The effect of the inner cylinder's number on the flow and heat transfer characteristics in porous media with several porosity and Darcy numbers and also the effect of nanoparticle's volume fraction were investigated.

The main conclusions of this work are as follows:

- For constant Darcy number and porosity coefficient, by increasing the Rayleigh number, the Nusselt number of the enclosure's cold wall increases. This is due to relatively better thermal performance of natural convection at high Rayleigh numbers.
- For constant Rayleigh number and porosity coefficient, by decreasing Darcy number, the Nusselt number of enclosure's cold wall decreases and the status of the flow changes in a way that diminishes thermal performance.
- For constant Darcy and Rayleigh numbers, by increasing the porosity coefficient, the Nusselt number of enclosure's cold wall increases. In addition, by increasing porosity coefficient, porous media effects on natural convection

decreases and the flow's status will be closer to the conditions without the presence of porous media.

- Assuming that the purpose in a specific geometry is natural convective heat transfer from warm surface cylinder to the container cold enclosure's wall (regarding average Nusselt number of cold enclosure's wall) and considering equal area for heat transfer of total warm surfaces in different geometries, using several cylinders with warm surfaces and lower radius's is better than using a single cylinder. It is worthy to note that, the arrangement of warm cylinders may affect the natural convective flow and heat transfer (not studied here).
- For constant porosity coefficient, Darcy number, and Rayleigh number, increasing the volume fraction of nanoparticles leads to better natural convective heat transfer.

To sum up, for improving heat transfer in nanofluid's natural convection between a cold square enclosure and an inner cylindrical pin-fins system filled with a homogeneous porous media, increasing Rayleigh number and volume fraction of nanoparticles is applicable. On the other hand, to control and decrease the related heat transfer, decreasing porosity coefficient and Darcy number is recommended. Moreover, using a geometry with several cylinders (instead of a single one) can be useful for heating the cold square enclosure.

ACKNOWLEDGEMENTS

We would like to show our gratitude to Dr. Mohammad Reza Salimi for sharing his view points with us during this research.

REFERENCES

Abu-Nada, E., Z. Masoud and A. Hijazi (2008). Natural convection heat transfer enhancement in horizontal concentric annuli using nanofluids. *International Communications in Heat and Mass Transfer* 35(5), 657-665.

Al-Amiri, A. (2000). Analysis of momentum and energy transfer in a lid-driven cavity filled with a porous medium. *Int. J. Heat Mass Trans.* 43(19), 3513-3527.

Alsabery, A. I., A. J. Chamkha, H. Saleh and I. Hashim (2017). Natural convection flow of a nanofluid in an inclined square enclosure partially filled with a porous medium. *Scientific Reports*, *7*(1), 1-18.

Arjun, K. S. and Kumar R. (2017). LBM analysis of micro-cConvection in MHD nanofluid flow. *Journal of Mechanical Engineering.* 63(7-8), 426-438.

Ashorynejad, H. R., M. Farhadi, K. Sedighi and A. Hasanpour (2012). Natural convection in a porous medium rectangular cavity with an applied vertical magnetic field using Lattice Boltzmann Method. *Applied Mechanics and Materials* 110, 839-846.

Bhatnagar, P. L., E. P. Gross and M. Krook (1954). A model for collision processes in gases. I. small amplitude processes in charged and neutral one-component systems. *Physical Review* 94(3), 511.

Brinkman, H. (1952). The viscosity of concentrated suspensions and solutions. *Journal of Chemical Physics* 20(4), 571-571.

Clague, D. S. and R. J. Phillips (1997). A numerical calculation of the hydraulic permeability of three-dimensional disordered fibrous media. *Physics of Fluids* 9(6), 1562-1572.

Dardis, O. and J. McCloskey (1998). Lattice Boltzmann scheme with real numbered solid density for the simulation of flow in porous media. *Phys. Rev. E* 57(4), 4834-4837.

Filippova, O. and D. H'anel (1998). grid refinement for lattice-BGK models. *J. Comput. Phys.* 147(1), 219-228.

Freed, D. M. (1998). Lattice-Boltzmann method for macroscopic porous media modeling. *Int. J. Mod. Phys. C* 9(8), 1491-1503.

Gartling, D. K., C. E. Hickox and R. C. Givler (1996). Simulation of coupled viscous and porous flow problems. *Comp. Fluid Dyn.* 7(1-2), 23-48.

Guo, Z. and T. S. Zhao (2002). Lattice Boltzmann model for incompressible flows through porous media. *Phys. Rev. E* 66(3), 036304-1-036304-9.

Guo, Z. and T. S. Zhao (2005). Lattice Boltzmann simulation of natural convection with temperature-dependent viscosity in a porous cavity. *Progress in Computational Fluid Dynamics* 5(1/2), 110-117.

Haghshenas, A., M. R. Nasr and M. Rahimian, (2010). Numerical simulation of natural convection in an open-ended square cavity filled with porous medium by lattice Boltzmann method. *International Communications in Heat and Mass Transfer* 37(10), 1513-1519.

Hasanpour, A., M. Farhadi, K. Sedighi and H. R. Ashorynejad (2012). numerical study of Prandtl effect on MHD flow at a lid-driven porous cavity. *International Journal for Numerical Methods in Fluids* 70(7), 886-898.

He, X., S. Chen and G. D. Doolen (1998). A novel thermal model for the lattice Boltzmann method in incompressible limit. *International Journal of Computational Physics* 146(1), 282-300.

Hickox, C. E and D. K. Gartling (1985). A numerical study of natural convection in a vertical annular porous layer. *Int. J. Heat Mass Trans* 28(3), 720-723.

Hsu, C. and K. Vafai (2005). Handbook of porous media. *CRC Press*, Taylor and Francis Group, Boca Raton.

Hsu, C. T. and P. Cheng (1990). Thermal dispersion in a porous medium. *Int. J. Heat Mass Trans* 33(8), 1587-1597.

Husseini, A. K., H. R. Ashorynejad, M. Sheikholeslami and S. Sivasankaran (2014). Lattice Boltzmann simulation of natural convection heat transfer in an open Enclosure filled with Cu–Water nanofluid in a presence of magnetic field. *Nuclear Engineering and Design* 268, 10-17.

Hwang, K. S., J. H. Lee and S. P. Jang (2007). Buoyancy-driven heat transfer of water-based Al2O3 nanofluids in a rectangular cavity. *International Journal of Heat and Mass Transfer* 50(19), 4003-4010.

Jafari, M., M. Farhadi, S. Akbarzade and M. Ebrahimi (2015). Lattice Boltzmann simulation of natural convection heat transfer of SWCNT-nanofluid in an open enclosure. *Ain Shams Engineering Journal*. 6(3), 913-927.

Jafari, Y., M. Taeibi-Rahni and A. Adamian (2015a). Numerical simulation the natural convective heat transfer of nano-fluid in porous media, using lattice-Boltzmann method. *The 14th Conference of Iranian Aerospace Society*, Iranian Scientific &Industrial Research Organization, Tehran, Iran (In Persian).

Jafari, Y., M. Taeibi-Rahni and A. Adamian (2015c). computational modeling of flow and Natural convective heat transfer in Porous media, using LBM- effects of nano-fluidicity and domain geometry. *Fluid Mechanics & Aerodynamics Journal* 3(4), 17-30 (In Persian).

Jafari, Y., M. Taeibi Rahni, P. Ramian and M. Haghshenas (2015b). The study of free convection heat transfer in porous media, for various circular geometries, using lattice Boltzmann method, *The 23rd International Annual Conference of Iranian Mechanical Engineering Society (ISME 2015)*, Department of Mechanical Engineering, Amirkabir University of Technology, Tehran, Iran, http://isme2015.aut.ac.ir/, 2015 (In Persian).

Kang, Q., D. Zhang and S. Chen (2002). unified lattice Boltzmann method for flow in multi-scale porous media. *Phys. Rev. E* 66(5), 056307-1–056307-11.

Karimipour, A. (2015). New correlation for Nusselt number of nanofluid with Ag / Al2O3 / Cu nanoparticles in a microchannel considering slip velocity and temperature jump by using lattice Boltzmann method. *International Journal of Thermal Sciences.* 93, 146-156.

Khanafer, K., K. Vafai and M. Lightstone (2003). Buoyancy-driven heat transfer enhancement in a two-dimensional enclosure, utilizing nanofluids. *International Journal of Heat and Mass Transfer* 46(19), 3639-3653.

Martys, N. S. (2001). Improved approximation of the Brinkman equation, using a lattice Boltzmann method. *Phys. Fluids* 13(6), 1807–1810.

Mei, R., L. S. Luo and W. Shyy (1999). An accurate curved boundary treatment in the lattice Boltzmann method. *Journal of Computational Physics* 155(2), 307-330.

Mohamad, A. A. (2011). Lattice Boltzmann method", *Springer*, London, UK.

Moukalled, F. and S. Acharya (1996). Natural convection in the annulus between concentric horizontal circular and square sylinders. *J. Thermophysics and Heat Transfer* 10(3), 524-531.

Nemati, H., M. Farhadi, K. Sedighi, E. Fattahi and A. A. R. Darzi (2010). Lattice Boltzmann simulation of nanofluid in lid-driven cavity. *International Communications in Heat and Mass Transfer*. 37, 1528–1534.

Nield, D. and A. Bejan (1999). Convection in porous media (2nd edn.). *Springer-Verlag*, New York, USA.

Nishimura, T., T. Takumi, M. Shiraishi, Y. Kawamura and H. Ozoe (1986). Numerical analysis of natural convection in a rectangular enclosure horizontally divided into fluid and porous regions. *Int. J. Heat Mass Trans.* 29(6), 889-898.

Nithiarasu, P., K. Seetharamu and T. Sundararajan (1997). Natural convective heat transfer in a fluid saturated variable porosity medium. *Int. J. Heat Mass Trans.* 40(16), 3955-3967.

NorAzwadi, C. and Siti A. R. (2014). Lattice Boltzmann Method for Convective Heat Transfer of nanofluids–A review. *Renewable and Sustainable Energy Reviews.* 38, 864-875.

NorAzwadi, C. and T. Tanahashi (2006). Simplified thermal lattice Boltzmann in incompressible limit. *International Journal of Modern Physics B.* 20(17), 2437-2449.

Rahmati, A. R., A. Rayat Roknabadi and M. Abbaszadeh (2016). Numerical simulation of mixed convection heat transfer of nanofluid in a double lid-driven cavity using lattice Boltzmann method. *Alexandria Engineering Journal.* 55(4), 3101-3114.

Salimi, M. R., M. Taeibi Rahni and F. Jam (2015a). Pore-scale simulation of fluid flow passing over a porously covered square cylinder located at the middle of a channel, using a hybrid MRT-LBM–FVM approach. *Theoretical and Computational Fluid Dynamics* 29(3), 171-191.

Salimi, M. R., M. Taeibi Rahni and F. Jam (2015b). New lifting relations for estimating LBM distribution functions from corresponding macroscopic quantities, based on equilibrium and non-equilibrium moments. *Journal of Computational Physics* 302, 155-175.

Salimi, M. R., M. Taeibi Rahni and F. Jam (2015c). Heat transfer analysis of a porously covered heated square cylinder, using a hybrid Navier–Stokes–lattice Boltzmann numerical method. *International Journal of Thermal Sciences* 91,

59-75.

Servati, V. A. A., K. Javaherdeh and H. R. Ashorynejad (2014).Magnetic field effects on force convection flow of a nanofluid in a channel partially filled with porous media using lattice Boltzmann method. *Advanced Powder Technology* 25(2), 666-675.

Seta, T., E. Takegoshi, and K. Okui (2006). Lattice Boltzmann simulation of natural convection in porous media. *Mathematics and Computers in Simulation* 72(2), 195-200.

Sheikholeslami, M., M. Gorji Bandpy and D. D. Ganji (2013a). Numerical investigation of MHD effects on Al2O3-water nanofluid flow and heat transfer in a semi-annulus enclosure using LBM. *Energy* 60, 501-510.

Sheikholeslami, M., M. Gorji Bandpy, S. M. Seyyedi, D. D. Ganji, H. B. Rokni and S. Soleimani (2013b). Application of LBM in simulation of natural convection in a nanofluid filled square cavity with curve boundaries. *Powder Technology* 247, 87-94.

Spaid, M. and F. R. Phelan (1997). Lattice Boltzmann methods for modeling microscale flow in fibrous porous media. *Phys. Fluids* 9(9), 2468–2474.

Spaid, M. and F. R. Phelan (1998). Modeling void formation dynamics in fibrous porous media with the lattice Boltzmann method. *Composites A* 29(7), 749–755.

Succi, S. (2001). *The lattice Boltzmann equation for fluid dynamics and beyond*. Oxford University Press Inc., New York, USA.

Sukop, M. C. and D. T. Thorne (2006) *Lattice Boltzmann modeling*. Springer, Berlin, Germany.

Tien, C. L. and K. Vafai (1989). Convective and radiative heat transfer in porous media. *Adv. Appl. Mech.* 27, 225–282.

Tomadakis, M. M. and T. J. Robertson (2005) Viscous permeability of random fiber structures: comparison of electrical and diffusional estimates with experimental and analytical results. *Journal of Composite Materials* 39(2), 163-188.

Varol, Y. (2012) Natural convection for hot materials confined within two entrapped porous trapezoidal cavities. *International Communications in Heat and Mass Transfer* 39(3), 282-290.

Wang, X. Q. and A. S. Mujumdar (2007). Heat transfer characteristics of nanofluids: a review, *International Journal of Thermal Sciences* 46(1), 1-19.

Xuan, Y. and Z. Yao (2005). Lattice Boltzmann model for nanofluids, *Heat Mass Transfer* 41, 199-205.

Yan, W. W., Y. Liu, Z. L. I. Guo and X. U. You-Sheng (2006). Lattice Boltzmann simulation on natural convection heat transfer in a two-dimensional cavity filled with heterogeneously porous medium. *International Journal of Modern Physics* 17(6), 771-783.

Yan, Y. Y. and Y. Q. Zu (2008). Numerical simulation of heat transfer and fluid flow past a rotating isothermal cylinder – A LBM approach. *Int. J. Heat Mass Trans.* 51(9-10), 2519-2536.

Zhao, C. Y., L. Dai, G. Tang, Z. Qu and Z. Li (2010). Numerical study of natural convection in porous media (metals), using lattice Boltzmann method (LBM). *International Journal of Heat and Fluid Flow* 31(5), 925-934.